

Interaction Notes

Note 606

May 2008

Deconvolution of a Conducting Sphere Scatterer Signature Using a Bistatic 6ft IRA Scene Simulated in WIPL-D

Mary C. Taylor and Tapan K. Sarkar

Syracuse University
Electrical Engineering and Computer Science Department
Syracuse, New York 13244

Abstract

The impulse radiating antenna (IRA) has been designed, analyzed, built and tested by E. Farr and others [3-12] in the years since it was first theorized by Carl Baum [1]. In this paper, a 6ft diameter IRA is modeled and two of them are used in a bistatic configuration along with a 20 inch diameter conducting sphere scatterer. The bistatic scene is simulated in the frequency domain using the electromagnetic analysis code WIPL-D [13]. Since the WIPL-D code uses entire domain basis functions over large subsectional patches it is possible to analyze electrically large antenna scattering scenes on a desktop computer utilizing modest computational resources. The greatest advantage of being able to simulate a practical antenna configuration using an electromagnetic analysis code is that the arrangement can be analyzed in a cost effective fashion using modest computational resources as opposed to using super computers and an elaborate measurement campaign which often becomes quite costly and time consuming. The objective of this document is to illustrate a process using deconvolution in the frequency domain to recover the time domain (and frequency domain) signature of the sphere scatterer from the simulated scene data. A system approach is used. First, in the time domain, the transmit and receive antenna contributions are decoupled and the late time pulse, due to the sphere scatterer, is isolated. Then, in the frequency domain, the individual transmit IRA and receive IRA signatures are deconvolved by division. The remaining response contains the combined signature of the input to the antenna and the scattering from the sphere. The input is a Gaussian pulse which behaves as a weighting on the frequency domain response of the scattering scene. This recovered response compares well with the simulated response of the sphere directly simulated with WIPL-D. In addition, a synthesis process convolving the simulated antennas, scatterer and input spectrums also shows good results, as expected.

This work was completed in the Computational Electromagnetics (CEM) Lab at Syracuse University with the support of the Air Force Research Laboratory, Directed Energy Directorate, Kirtland AFB, New Mexico, through ITT.

1. OUTLINE OF THE ANALYSIS PROCESS USED IN THIS PAPER:

The following five steps outline the analysis process which is detailed in this document.

1. Model and simulate an IRA based on a Farr Research design [3], but using a 6 ft diameter reflector and 45° feed arms, using the electromagnetic analysis code WIPL-D.
2. Model and simulate a scene consisting of a pair of 6 ft IRAs in a bistatic configuration with a 20 inch diameter sphere scatterer and no ground plane. Repeat the simulation with the antennas only and no sphere scatterer. In addition, simulate each component of the scene individually: the transmit (Tx) IRA alone, the receive (Rx) IRA alone, and the sphere scatterer alone. The location and orientation of the components simulated alone is the same as in the full scene simulation.
3. Post processing of the frequency domain responses obtained from WIPL-D into time domain by weighting the frequency domain data by a Gaussian window and implementing the inverse discrete Fourier transform (IDFT) through Matlab.
4. Recover the windowed sphere scatterer frequency domain signature in three steps. First, in the time domain, subtract the response of the scene without the scatterer from the response with the scatterer to remove the antenna couplings from the late time pulse. Second, isolate the subtracted late time pulse from remnants of the early time antenna coupling, and transform it back to the frequency domain using a discrete Fourier transform (DFT). Third, in the frequency domain, deconvolve the antenna contribution by dividing out the frequency domain signatures of the Tx IRA and Rx IRA simulations. This recovered windowed spectrum can be compared to the simulated sphere spectrum, after the same Gaussian window is applied.
5. Recover the sphere scatterer time domain signature by transforming (IDFT) the recovered windowed frequency domain sphere response back to the time domain. This time signature is compared to the time domain signature of the sphere alone, which has been simulated separately in WIPL-D.

As an additional check, we synthesize the frequency domain response for the late time pulse and compare this to the late time response results from the full scene simulation.

This work has been completed in the Computational Electromagnetics (CEM) Lab at Syracuse University with the support of the Air Force Research Laboratory, Kirtland AFB, through ITT to investigate the performance of a reflector-type impulse-radiating antenna using computational electromagnetic modeling and simulation.

2. PHYSICAL DESCRIPTION OF THE IRA MODEL AND THE SCENE:

The IRAs used in this analysis are based on E. Farr’s IRA-2 design [3], except the feed arms are at 45° instead of 30° and the reflector diameter is 6ft instead of 46cm. Results for a 46cm IRA with 45° feed arms and the details of the analysis are available in a previous report by the authors [2]. Therefore, a brief summary of the IRA model will be given and then this report will focus on the use of this 6ft IRA in the scene.

TABLE 1: List of symbols used to describe the parameters of the IRA and their values

Symbol	[meters]	Parameter	Description
D	1.83	given	Diameter of the Paraboloidal Reflector Aperture
F/D	0.4	given	Ratio of Focal Length to Aperture Diameter [unitless]
L/D	0.4	given	Ratio of Feed Arm Sphere Radius to Aperture Diameter
Calculated			
R	0.92	=D/2	Radius of Paraboloidal Reflector Aperture
F	0.73	=(F/D)*D	Focal Length
L	0.73	=(L/D)*D	Radius of Feed Arm Sphere
d	0.29	= $R^2/(4*F)$	Depth of Paraboloidal Reflector
L_A	1.02	= $\sqrt{(F-d)^2+R^2}$	Length from Focal Point to Reflector Rim
Angle from axis	[radians]	[degrees]	
Beta_1	0.92	52.46	= $\arccos[(F-d)/F]$ (or = $\arcsin[\sqrt{(F^2-(F-d)^2)}/F]$)
Beta_0	1.12	64.01	= $\arccos[(F-d)/L_A]$ (or = $\arcsin[(R)/L_A]$)
Beta_2	1.32	75.57	= Beta_0 + Delt20
Included Angle			
Delt01	0.20	11.56	= Beta_0 - Beta_1
Delt20	0.20	11.56	= Delt01
Delt21	0.40	23.11	= Delt20 + Delt01

A parametric model for the IRA has been developed in WIPL-D using the values shown in Table 1. The advantage of using a parametric representation of the structure is that it is easily scaled for optimization. To allow for maximum scalability of the model, only three parameters: D, F/D and L/D, were assumed as “given” and all the other values are derived from these three parameters. Figure 1 shows two views of the IRA as modeled in WIPL-D using y-axis symmetry (x0z plane).

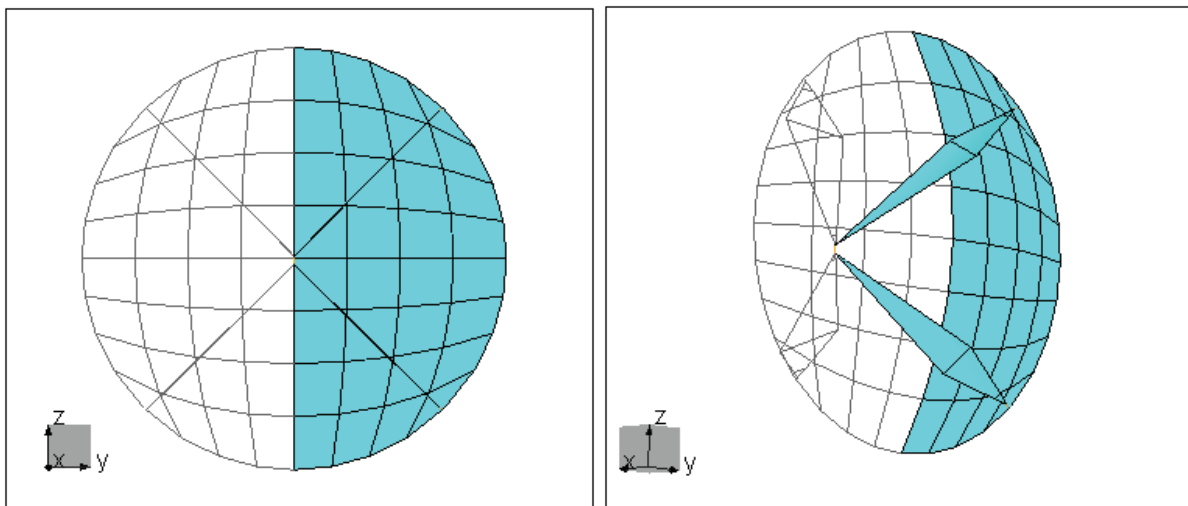


Figure 1 Two views of the 6 ft diameter IRA with 45° feed arms modeled in WIPL-D.

Two IRAs are placed 15 m from the origin in a bistatic configuration with the Tx IRA located along the x axis and tilted upward toward the front and center of a sphere scatterer located 3.94 ft (1.2m) above the origin. No ground plane was used in this investigation. The Rx IRA is located 3 ft (0.915m) above the Tx IRA and it is also tilted downward toward the front and center of the sphere scatterer. The scatterer is a PEC sphere of 20 inch (0.508m) diameter.

Figure 2 depicts the dimensions and orientation of the components assembled in the scene.

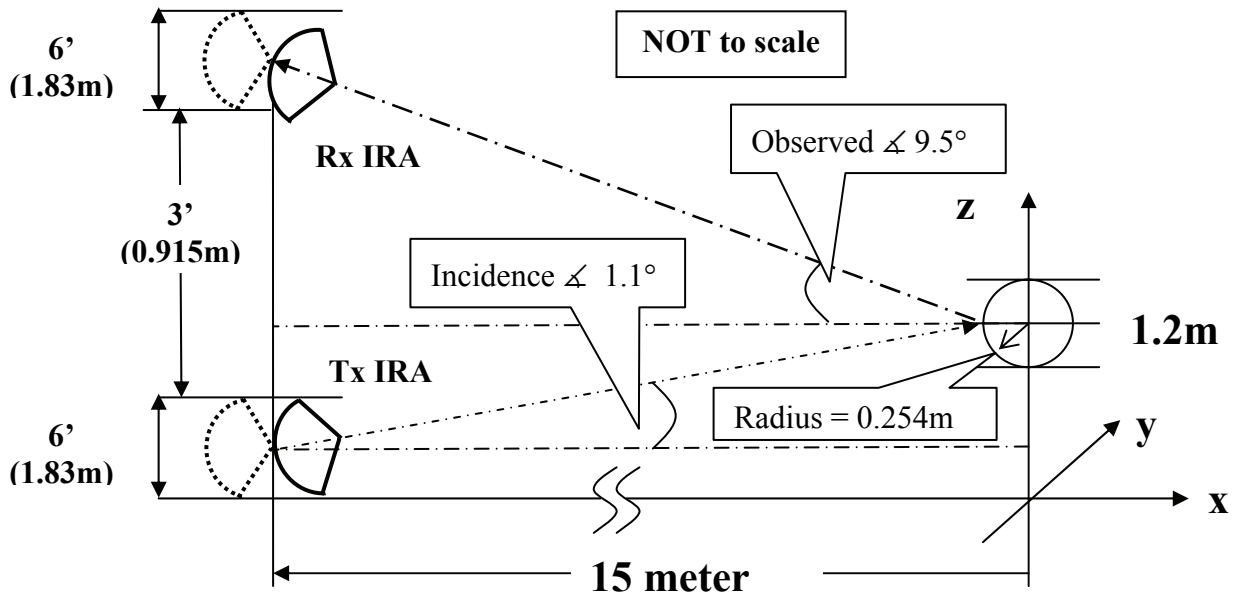


Figure 2 Diagram of bistatic scene with Tx and Rx IRAs and sphere scatterer (not to scale)

3. SYSTEM DESCRIPTION FOR RECOVERING THE SCATTERER SIGNATURE:

To recover the time domain (TD) and frequency domain (FD) scatterer signature, a system approach is used. Recognize that the antennas and the scatterer form a system which operates on the input to the transmitter and results in the output response at the receiver. However, there is a component of mutual coupling between the two antennas that adds to the complexity of the system model, even though the contribution is small due to the high directivity of IRAs.

The following development uses continuous time t and continuous radian frequency ω , even though the actual computations are in discrete frequency and time. A general system representation is shown below; where $x_i(t)$ is the input, $h_F(t)$ is the impulse response (or system operator) of the full scene and $y(t)$ is the output. The block diagram below is equivalent to the equation $y(t) = x_i(t) \otimes h_F(t)$, where the symbol \otimes denotes convolution.

$$x_i(t) \rightarrow \boxed{h_F(t)} \rightarrow y(t)$$

The full scene impulse response $h_F(t)$ consists of the individual transmitter $h_T(t)$, receiver $h_R(t)$ and scatterer $h_S(t)$ impulse responses. Expanding $h_F(t)$, we get the diagram below.

$$x_i(t) \rightarrow \boxed{h_T(t)} \rightarrow \boxed{h_S(t)} \rightarrow \boxed{h_R(t)} \rightarrow y(t)$$

In the bistatic antenna configuration there is mutual coupling, which is the leakage of the transmitter output directly to the receiver. This coupling gives the early time response and includes no influence from the scatterer, since the response at the Rx is observed before the Tx output has had time to travel to the scatterer and return to the Rx. This coupling can be modeled as

$$x_i(t) \rightarrow \boxed{h_T(t)} \rightarrow \begin{array}{c} \bullet \\ \downarrow \\ \boxed{\tau_{TS}} \rightarrow \boxed{h_S(t)} \rightarrow \boxed{\tau_{SR}} \rightarrow \bullet \\ \uparrow \\ \boxed{h_R(t)} \end{array} \rightarrow y(t)$$

where $\tau_{TS} = d_{TS}/c$ is the time delay for the Tx output to travel to the scatterer and $\tau_{SR} = d_{SR}/c$ is the time delay for the backscattered field to travel to the Rx ($c = 3 \times 10^8$ m/s, speed of light).

To simplify, the output can be modeled as two components $y(t) = y_E(t) + y_L(t)$ where $y_L(t)$ is the late time component due to the scatterer:

$$y_L(t) = x_i(t) \otimes h_T(t) \otimes h_S(t) \otimes h_R(t)$$

and $y_E(t)$ is the early time component due to antenna mutual coupling:

$$y_E(t) = x_i(t) \otimes h_C(t)$$

which add together as shown below.

$$x_i(t) \rightarrow \begin{array}{c} \bullet \\ \downarrow \\ \boxed{h_T(t)} \rightarrow \boxed{h_S(t)} \rightarrow \boxed{h_R(t)} \\ \uparrow \\ \oplus \end{array} \rightarrow y(t)$$

$$\quad \quad \quad \boxed{h_C(t)}$$

An expression in the frequency domain can be written for the above system representation as

$$X_i(\omega)H_T(\omega)H_S(\omega)H_R(\omega) + X_i(\omega)H_C(\omega) = Y(\omega)$$

where:

$$\begin{aligned} X_i(\omega) &\xleftrightarrow{\mathfrak{F}} x_i(t), & H_T(\omega) &\xleftrightarrow{\mathfrak{F}} h_T(t), & H_S(\omega) &\xleftrightarrow{\mathfrak{F}} h_S(t) \\ H_R(\omega) &\xleftrightarrow{\mathfrak{F}} h_R(t), & H_C(\omega) &\xleftrightarrow{\mathfrak{F}} h_C(t), & Y(\omega) &\xleftrightarrow{\mathfrak{F}} y(t) \end{aligned}$$

where \mathfrak{F} indicates the Fourier transforms of the corresponding continuous time signals.

To isolate and recover the frequency response of the scatterer, we solve for $H_S(\omega)$

$$H_S(\omega) = \frac{Y(\omega) - X_i(\omega)H_C(\omega)}{X_i(\omega)H_T(\omega)H_R(\omega)} = \frac{Y_L(\omega)}{X_i(\omega)H_T(\omega)H_R(\omega)}$$

which is valid for $X_i(\omega)$, $H_T(\omega)$ and $H_R(\omega) \neq 0$.

The development presented in this section offers an overview of the general theory applied in this paper. Actually, the process used in this investigation starts with the frequency domain data, as simulated by the electromagnetic analysis code WIPL-D. The next step is to transform the frequency domain data to the time domain for removal of the mutual coupling component and isolation of the late time response. Then, a transformation back to the frequency domain of just the isolated late time response due to the scatterer simplifies the deconvolution step. To minimize error due to division by zero (and small numbers close to zero), we leave the frequency domain scatterer signature in the form $H_S(\omega)X_i(\omega)$. The next three sections follow this process and present the data and results of this analysis.

4. COMPUTE ELECTROMAGNETIC IMPULSE RESPONSE:

The electromagnetic analysis code WIPL-D is used to compute the electromagnetic response of the scene. WIPL-D computes the electromagnetic response vs. frequency for antenna and scattering operations. The response is computed at discrete frequencies and for a range and step size as specified in the project parameters. For the signal processing of this frequency domain data, a Gaussian input function is used: $x_i(t) = x_g(t)$. Although the computations extend to a finite maximum frequency, the procedure described in the previous section essentially multiplies the frequency domain results of the WIPL-D simulation with a Gaussian windowing function in frequency: $\tilde{H}(\omega)X_G(\omega) = H(\omega)$, where $X_G(\omega) \xleftrightarrow{\mathfrak{F}} x_g(t)$. This is equivalent to a time domain convolution of a Gaussian input pulse with the time domain response of the simulation: $\tilde{h}(t) \otimes x_g(t) = h(t)$. The result of the windowing is a frequency response that smoothly transitions to zero. This windowing operation ensures that additional frequency components which are not present in the simulated response do not get introduced in the post-processing. The WIPL-D results, although limited in frequency, mimic an infinite frequency response after this windowing operation. Therefore, consistent with the explanation in the previous section, these WIPL-D results will be referenced to their corresponding impulse response designations.

Five WIPL-D simulation projects were run for this investigation: the complete scene, the mutual coupling of the antennas only - no sphere scatterer, the Tx IRA alone, the Rx IRA alone, and the sphere scatterer alone. The location and orientation of the component simulated alone was the same as in the full scene. All simulations used the same frequency parameters summarized below.

Start Frequency	5 MHz
Stop Frequency	2 GHz
Frequency Step	5 MHz
Number of Frequencies	400

The frequency domain results of the five simulations are shown in Figures 3 through 8.

First, the response of the complete scene, consisting of the input, the transmitter, the sphere scatterer and the receiver, is shown. This response corresponds to $H_F(\omega) \xleftrightarrow{S} h_F(t)$, as presented in Section 3. Figure 3a plots the magnitude of the complex current on the central input wire of the Rx IRA. The current on the Rx IRA is proportional to the electromagnetic radiation incident on the receiver wire due to a delta generator source $E_G = 1V$ at the feed point of the Tx IRA and backscattered from the sphere, located at the origin and 15m away from the antenna pair. Figure 3b shows the real and imaginary components.

Second, the impulse response of the mutual coupling scene, consisting of the input, the transmitter and the receiver, is presented. This response corresponds to $H_C(\omega)$, as presented in Section 3. Figure 4a plots the magnitude of the complex current on the central input wire of the Rx IRA. This current is proportional to the electromagnetic radiation incident on the receiver wire due to a delta generator source $E_G = 1V$ at the feed point of the Tx IRA and transmitted directly to the Rx IRA. Figure 4b shows the real and imaginary components.

Figure 5 overlays the spectrums of the scene with and without the scatterer. The presence of the scatterer at the origin results in a modulation of the response, which is consistent with a delay in time. Figure 5b zooms in for a closer look at the modulation. The fact that the chosen frequency step of 5 MHz cannot accurately capture this modulation may account for some of the error in the results. Future work will simulate the scene with a finer frequency step to identify if improvements in the results can be seen.

Third, the impulse response of the Tx IRA, which corresponds to $H_T(\omega)$, is shown. The Tx IRA is alone, with a delta generator source $E_G = 1V$ at the feed point. Figure 6 plots far field radiation E_θ observed at an angle of 1.11° (magnitude in 6a, complex in 6b).

Fourth, the impulse response of the Rx IRA, which corresponds to $H_R(\omega)$, is shown. The Rx IRA alone and at the same location and tilt angle as in the complete scene. A vertically polarized plane wave of $E_\theta = 1V/m$ and at an angle of 9.5° is incident on the Rx IRA. Figure 7 plots the current on the wire at the center point of the IRA where the four arms connect (magnitude in 7a, complex in 7b).

Lastly, the radar cross section vs. frequency of the sphere scatterer, which corresponds to $H_S(\omega)$, is shown. The sphere is in the same location above the origin, as in the full scene. A vertically polarized plane wave of $E_\theta = 1V/m$ is incident at an angle of 1.11° . Figure 8 plots the backscattered far field E_θ observed at an angle of 9.5° (magnitude 8a, complex 8b).

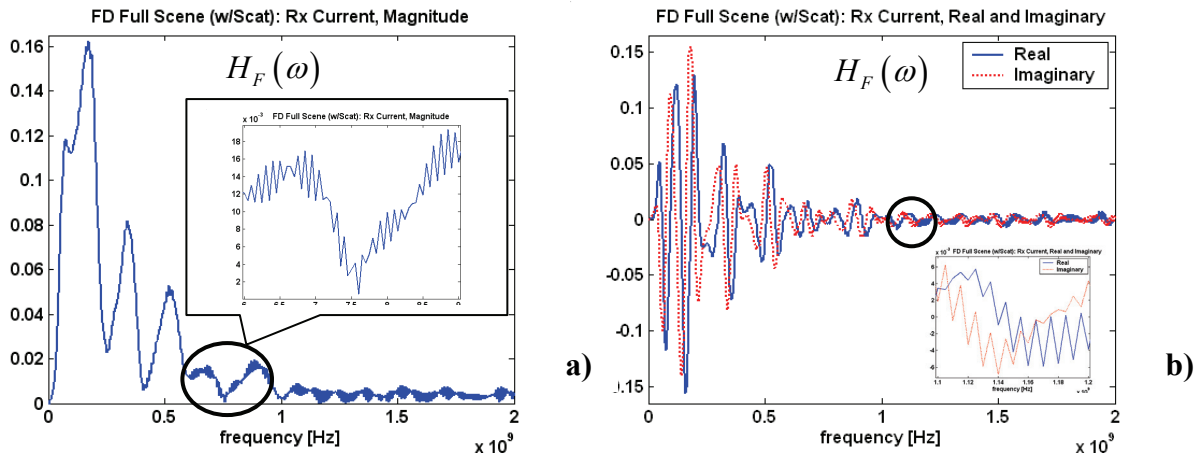


Figure 3 The Full Scene, Rx IRA Current: a) Magnitude, b) Real and Imaginary

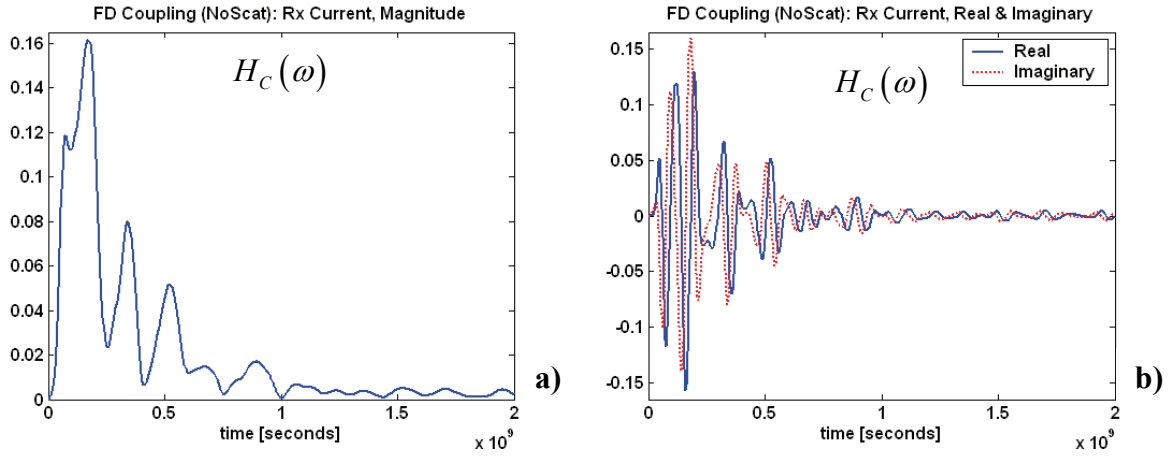


Figure 4 Antenna Coupling only, Rx IRA Current: a) Magnitude, b) Real and Imaginary

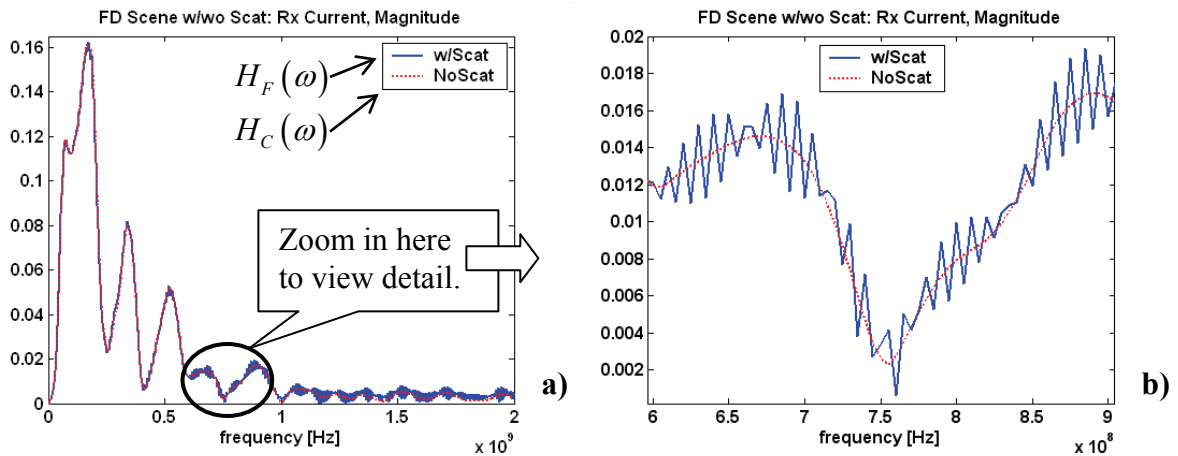


Figure 5 Overlay Frequency Domain Response, Scene w/wo Scatterer: a) full range, b) zoom

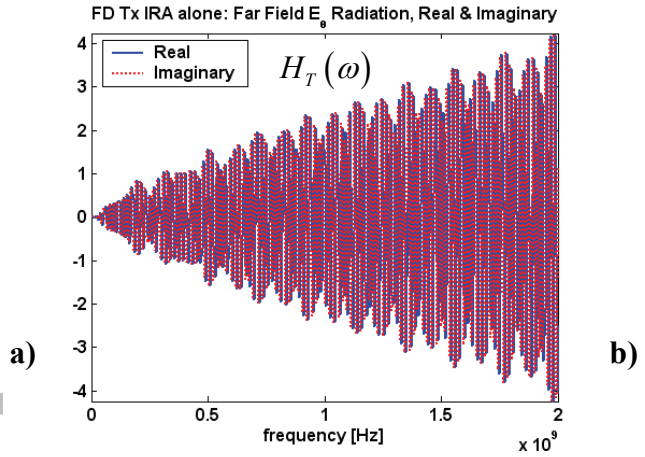
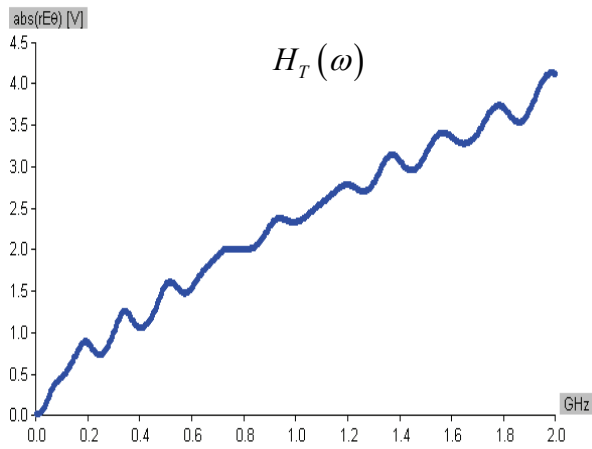


Figure 6 Tx IRA alone, Far Field Radiation, E_θ : a) Magnitude from WIPL-D, b) Complex

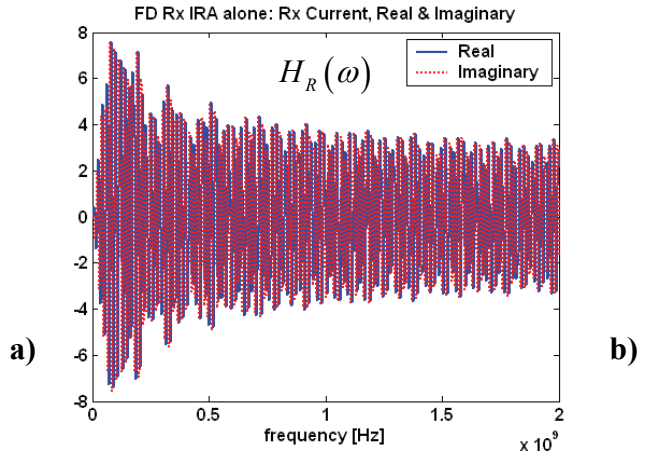
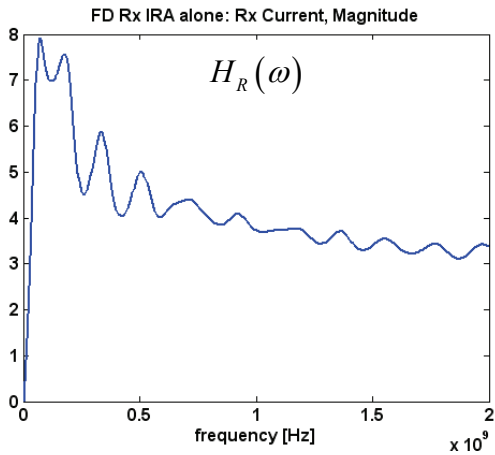


Figure 7 Rx IRA alone, Current on central wire: a) Magnitude, b) Real and Imaginary

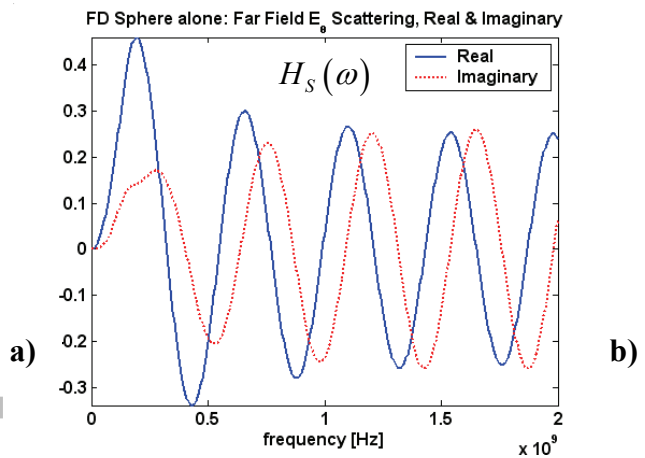
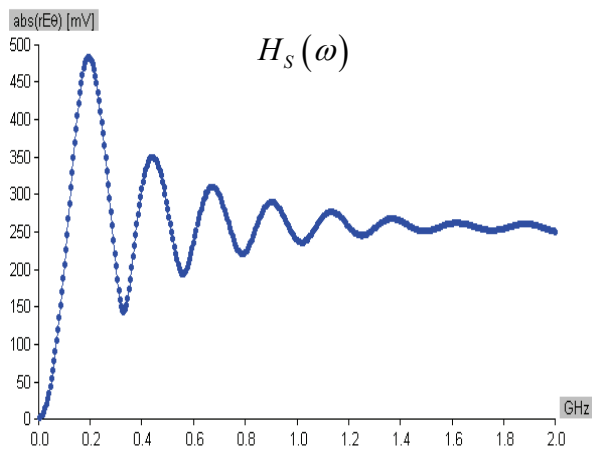


Figure 8 Sphere Scatterer, Far Field Scattering, E_θ : a) Magnitude from WIPL-D, b) Complex

5. TRANSFORM FREQUENCY DOMAIN DATA TO TIME DOMAIN:

To transform the frequency domain (FD) results simulated in WIPL-D to the time domain (TD), the process outlined below is followed. The process is described and accompanied by nine plots of the processing of the Tx IRA alone from FD to TD.

First, we bring the real and imaginary FD data set into Matlab and plot Figure 9a to verify agreement with the WIPL-D data $H_T(\omega)$, shown in Figure 6a. The signal processing parameters selected and calculated for the analysis are summarized in Table 2 below. Next, we extend the length of the FD data to the sequence period length N , insert the conjugate symmetric values and zero pad the remainder, which results in the plot shown in Figure 9b.

TABLE 2: List of signal processing parameters

Parameter		Value	Description
Δf	set by simulation	5 MHz	frequency spacing or frequency resolution
N	select	$2^{10} = 1024$	sequence period (min 2 x no. of freq samples)
f_s	calc: $f_s = N\Delta f$	5.12 GHz	sampling frequency (min 2x highest freq)
Δt	calc: $\Delta t = 1/f_s$	195.3 psec	sampling interval or time resolution
T_0	calc: $T_0 = 1/\Delta f$	200 nsec	record length (duration of TD signal)

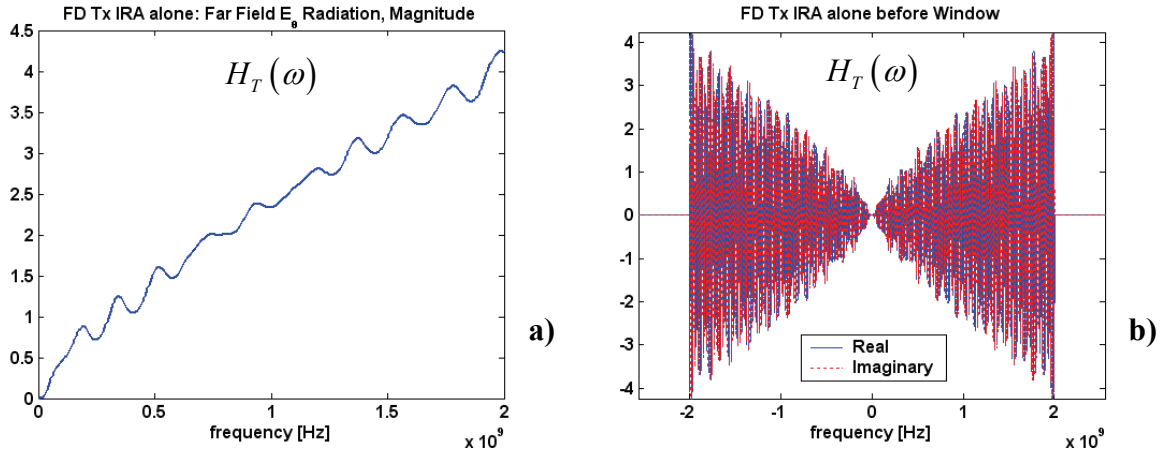


Figure 9 Tx IRA alone, Far Field Radiation E_0 : a) Magnitude – compare to Figure 6a, b) Real and Imaginary with Conjugate Symmetry and Zero Padding – compare to Figure 6b

A Gaussian input pulse is defined in the time domain and is then Fourier transformed.

$$g(t) = e^{-\gamma^2}; \quad \gamma = \frac{2}{T}(t - t_0), \quad T = 1n \text{ sec}, \quad t_0 = 20n \text{ sec}$$

$$G(\omega) = \mathfrak{F}\{g(t)\} = \frac{T\sqrt{\pi}}{2} e^{-\left(\frac{T\omega}{2}\right)^2} e^{-j\omega t_0}$$

The Gaussian window is shown in Figure 10, with a bandwidth of approximately 2 GHz and an initial time delay of 20nsec. The FD data is multiplied by the Gaussian window, with the result plotted in Figure 11. Taking the Inverse Discrete Fourier Transform (IDFT) of this result gives the Time Domain Response, shown in Figure 12. This process is repeated for each of the five frequency data sets from WIPL-D and the results are plotted in Figures 13 – 17.

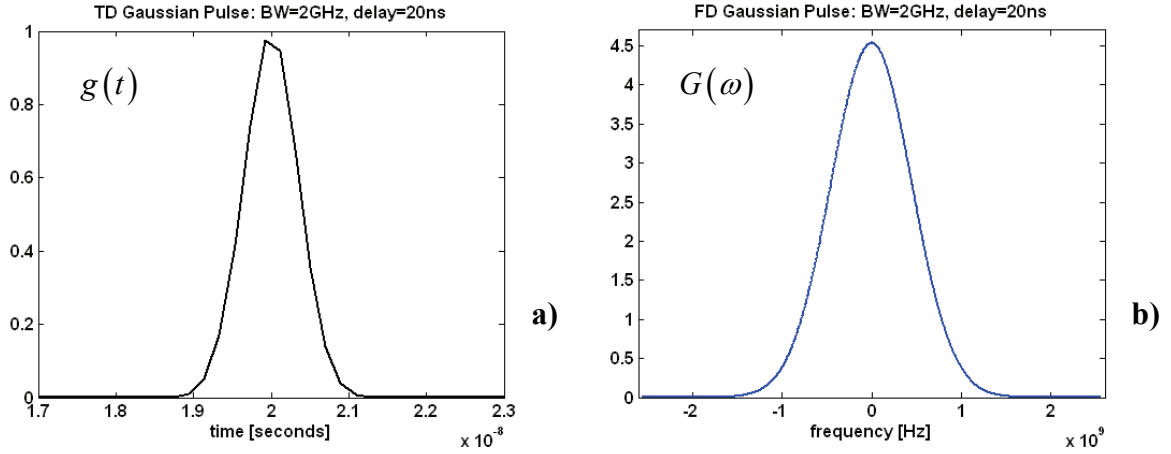


Figure 10 The Gaussian Window a) Time Domain $g(t)$, b) Frequency Domain $G(\omega)$

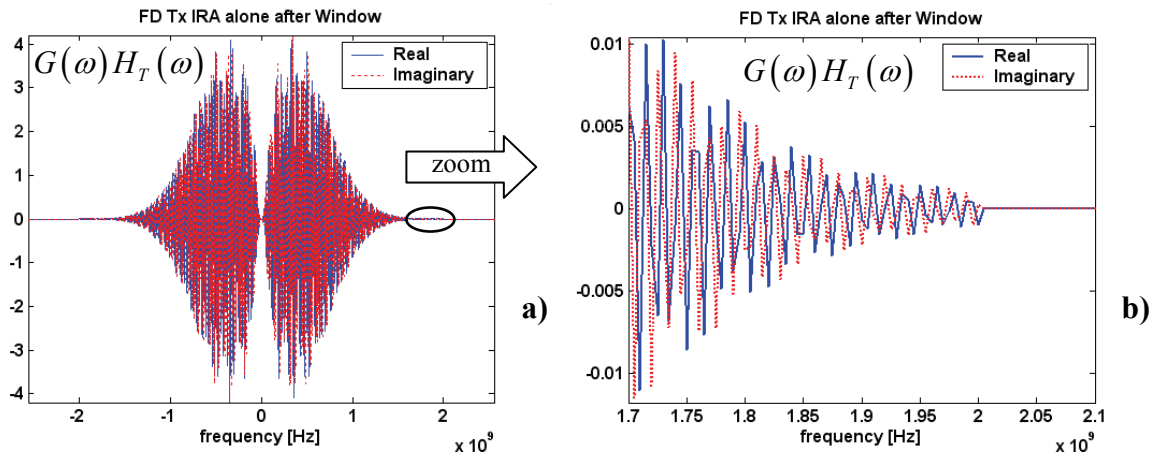


Figure 11 The Windowed FD data, before IDFT: a) full extent, b) zoom in around 2 GHz

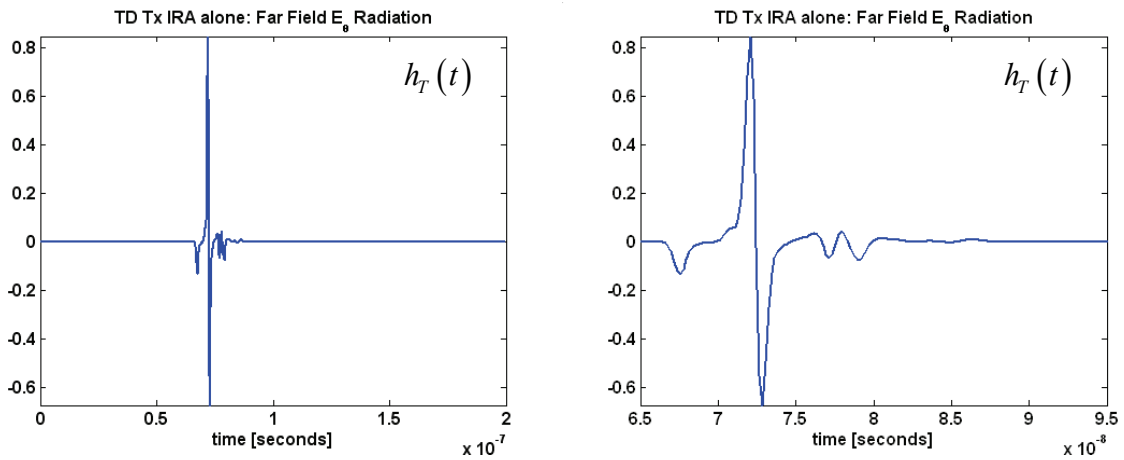


Figure 12 Tx IRA alone, Time Domain: a) full extent, b) zoom in on feature

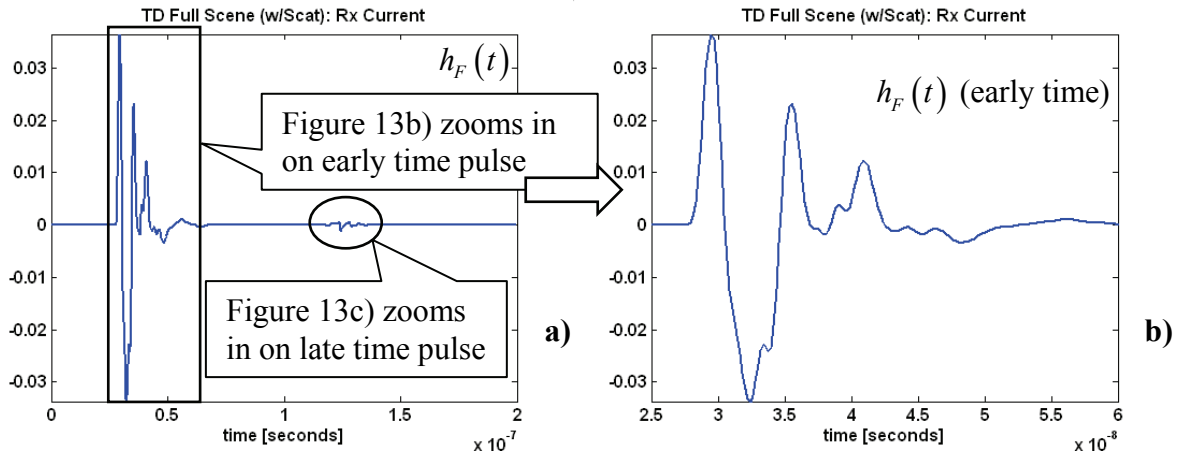


Figure 13 Complete Scene Time Domain: a) full extent, b) zoom on early time pulse

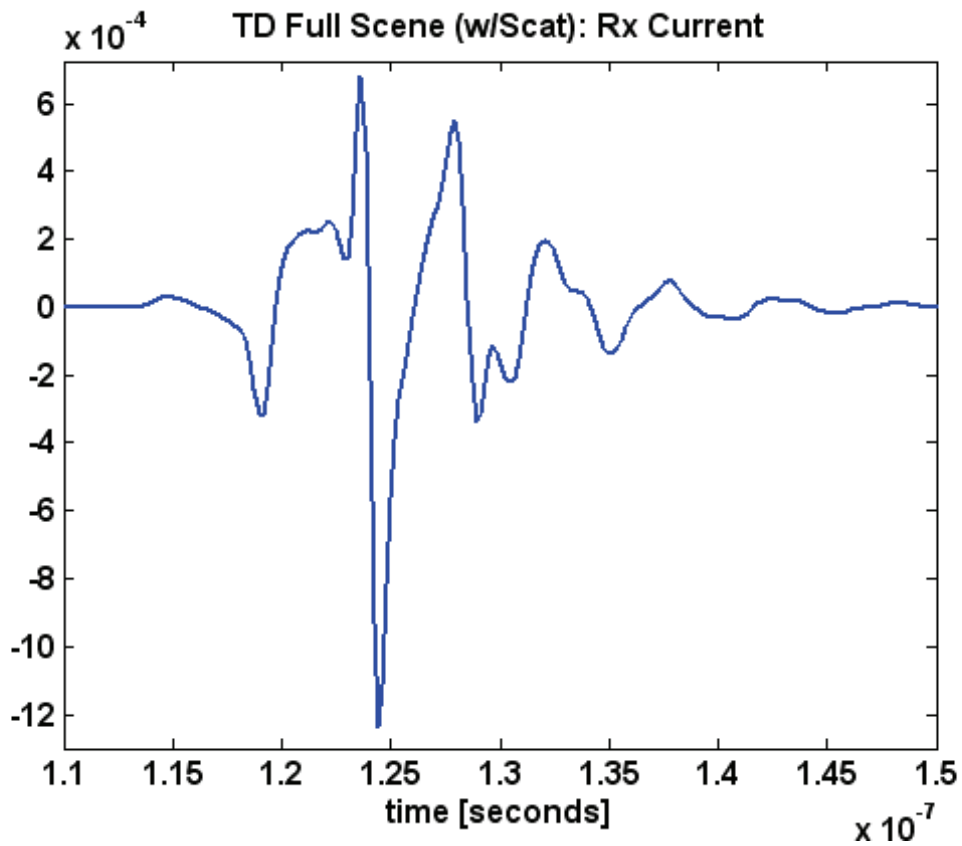


Figure 13 c) Complete Scene Time Domain: zoom in on Late Time Pulse due to scatterer

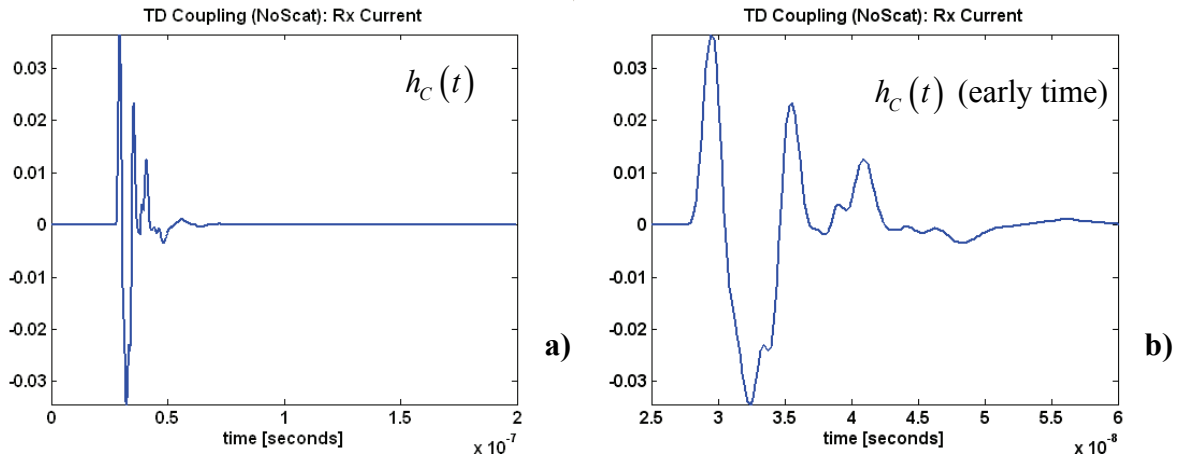


Figure 14 Antenna Coupling, Scene w/No Scatterer: a) full extent, b) zoom in on early time

Figure 14c)
 No Late Time Pulse
 is present, although
 there is a very small
 remnant of the early
 time response

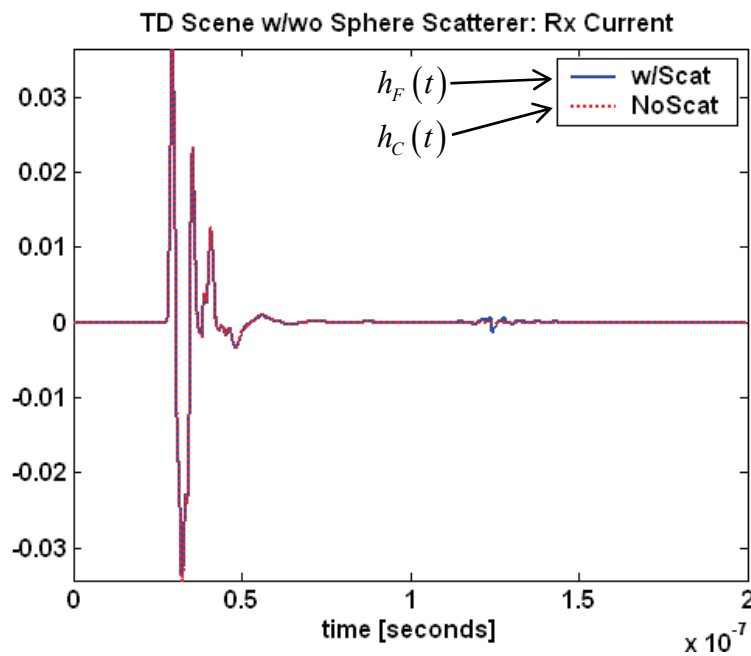
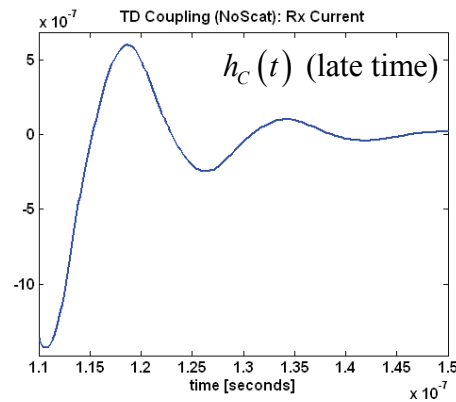


Figure 15 Overlay Time Domain Response, Scene w/wo Sphere Scatterer

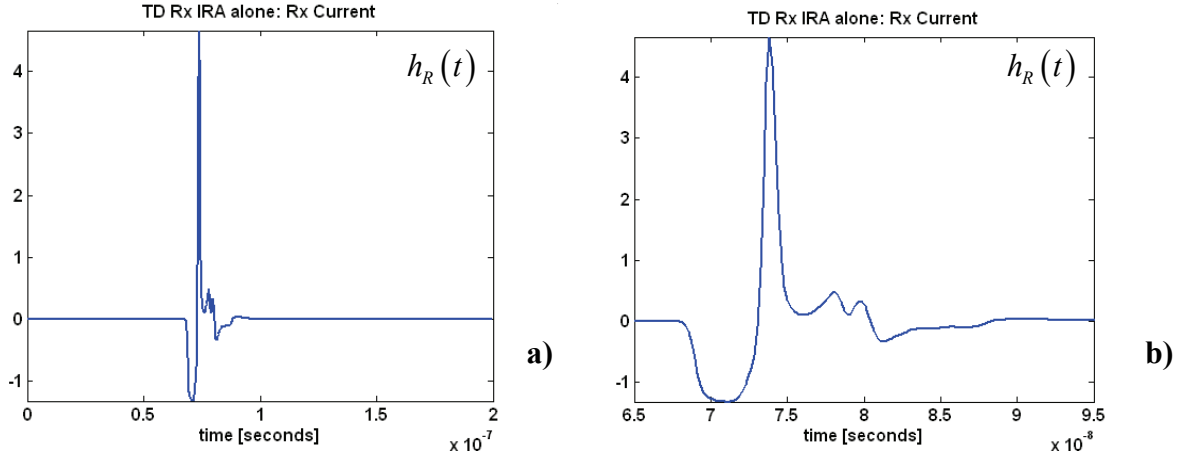


Figure 16 Receive IRA alone, Time Domain: a) full extent, b) zoom in on signal features

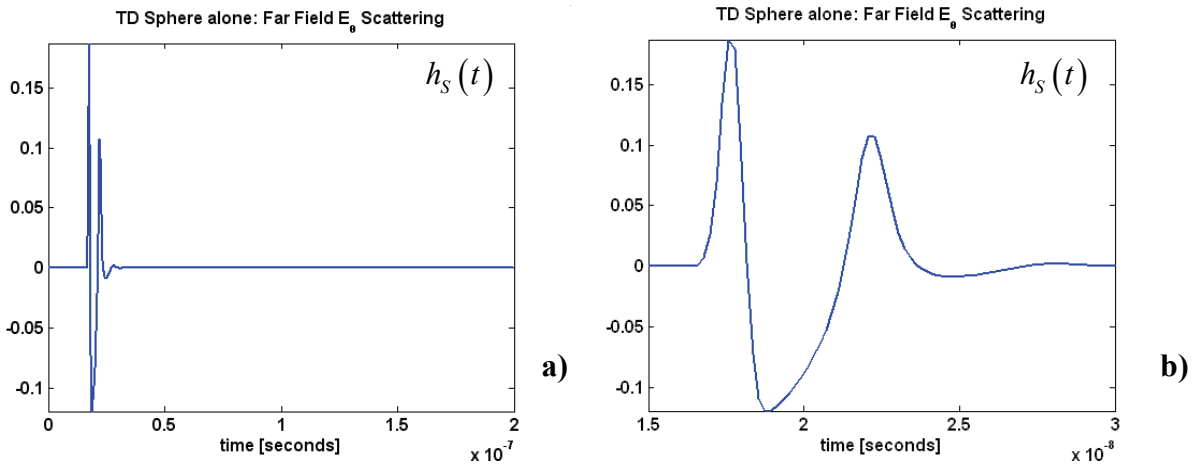


Figure 17 Sphere Scatterer alone, Time Domain: a) full extent, b) zoom in on signal features

6. RECOVER SPHERE SCATTERER SIGNATURE, FD AND TD:

Figures 18 – 26 illustrate the process described in Section 3 to recover the scatterer signatures. Figure 18a is the result of subtracting the time domain response of the scene without the scatterer, shown in Figure 14, from the response of the scene with the scatterer, shown in Figure 13. In Figure 18a, there is a significantly suppressed remnant of the early time pulse which survives the subtraction operation. This is because the two discrete time signals are very close, but they do not perfectly overlap due to numerical errors. This early time remnant is removed from further analysis by replacing the discrete values with zeros. Figure 18b zooms in on the start of the late time pulse to highlight the point at which the non-zero values are set to zero. The isolated late time pulse has been shown previously in Figure 13c.

Figure 19 is $Y_L(\omega)$ the Fourier transform of the isolated late time response. To find the desired $X_i(\omega)H_S(\omega)$, we first multiply the Tx IRA and Rx IRA spectrums, which are shown separately in Figures 6 and 7, respectively. Figure 20a plots the normalized $H_T(\omega)$ and $H_R(\omega)$ along with their product. The deconvolution of the antennas from the output is

accomplished in the frequency domain by division. Figure 20b overlays the product $H_T(\omega)H_R(\omega)$ with the output $Y(\omega)$ and the recovered quantity $X_i(\omega)H_S(\omega)$, which is the result of the division. Recall that $X_i(\omega)H_S(\omega)$, shown in Figure 20c, is the recovered frequency domain signature of the sphere scatterer convolved with the Gaussian input pulse. Figure 21 zooms in on the results shown in Figure 20 to highlight the data points close to zero frequency where the deconvolution is not valid due to division by zero. A total of three data point were interpolated to allow continuation of the recovery process.

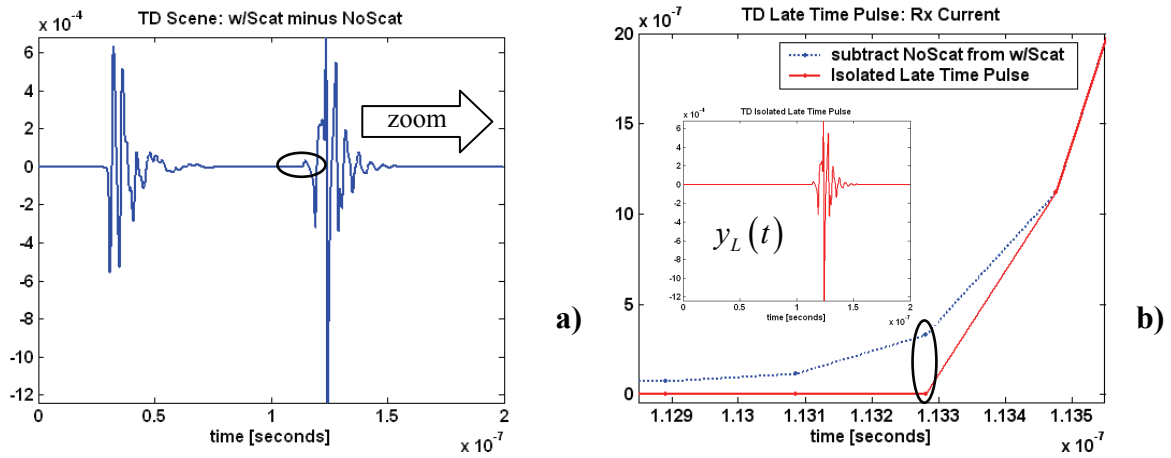


Figure 18 The Late Time Pulse: a) after subtraction, includes remnant of the early time pulse, b) zoom in on the start of the late time pulse, signal remnant prior to the start is set to zero

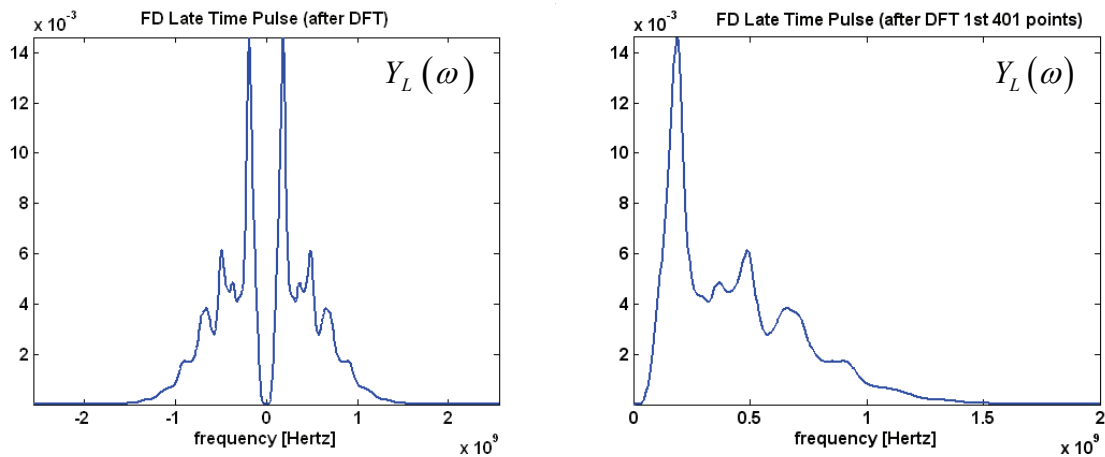


Figure 19 Spectrum of the Late Time Pulse: a) full spectrum, b) first 401 points after DFT

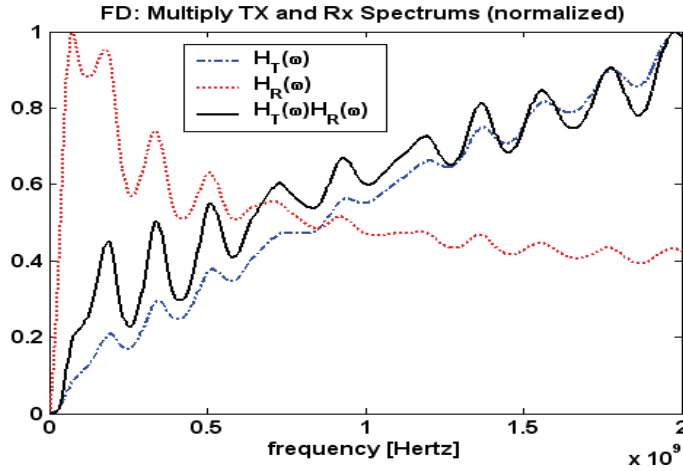


Figure 20 a) Deconvolution: Normalized Tx and Rx Spectrums overlaid with their product

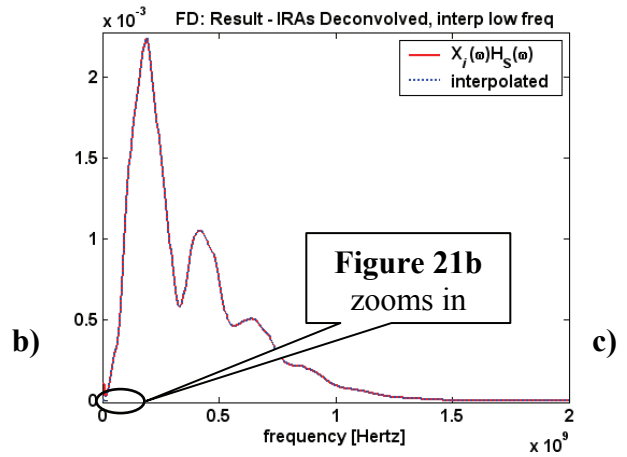
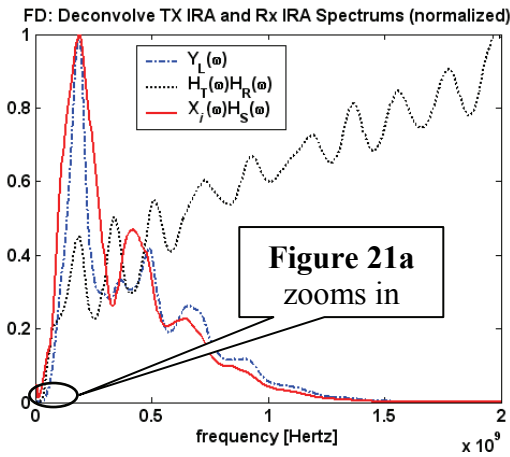


Figure 20 Deconvolution: b) Overlay Normalized Spectrums, c) Result after Deconvolution

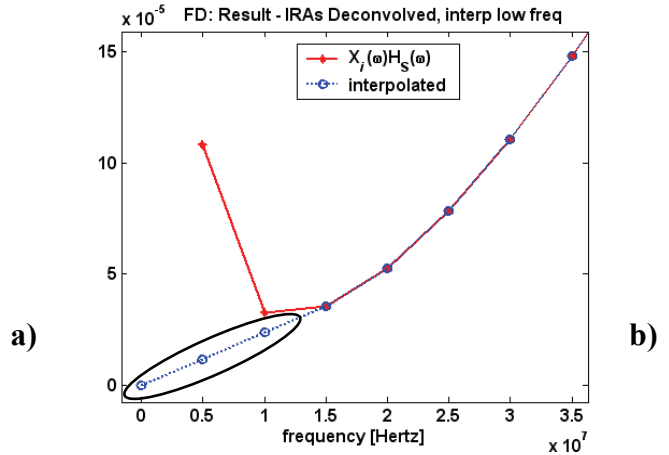
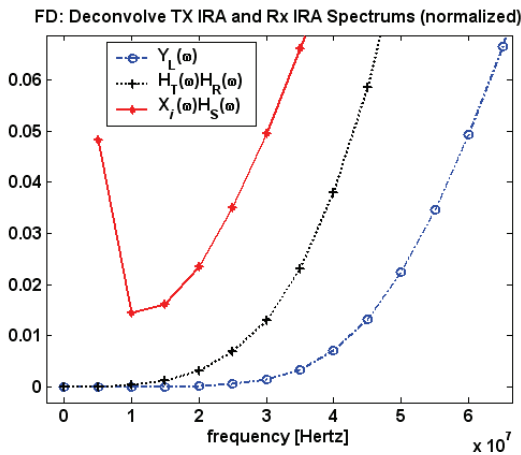


Figure 21 Zoom in on Deconvolved Spectrum at zero freq: a) values close to zero blow up b) Set DC value to zero and interpolate the first two data points for a smooth transition

At this point, we can compare the deconvolved frequency domain signature of the sphere with input to the frequency results from WIPL-D of a simulated sphere alone as a scatterer. First, the WIPL-D simulated scattering vs. frequency data must be convolved with the Gaussian input pulse, so that we are comparing like signals. The same Gaussian input pulse shown in Figure 10 is used, with a width of 1 nsec (approximately 2GHz in frequency) and a delay of 20 nsec. Multiplication in the frequency domain provides the result, plotted in Figure 22, overlaid with the raw data from WIPL-D, previously plotted in Figure 8. Figure 23 overlays the recovered signature with this windowed result. Good agreement is achieved.

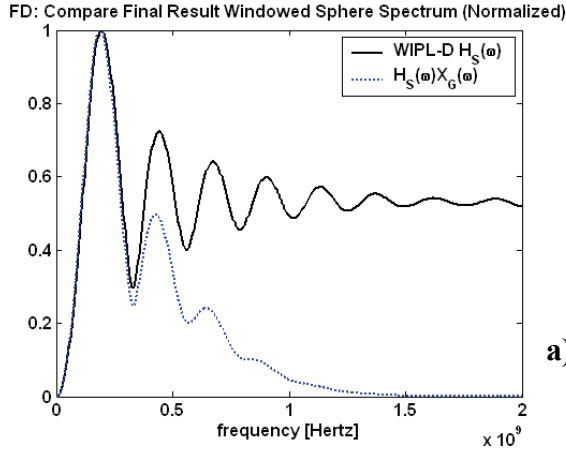


Figure 22 Spectrum of Simulated Sphere with/without the Gaussian Input (window)

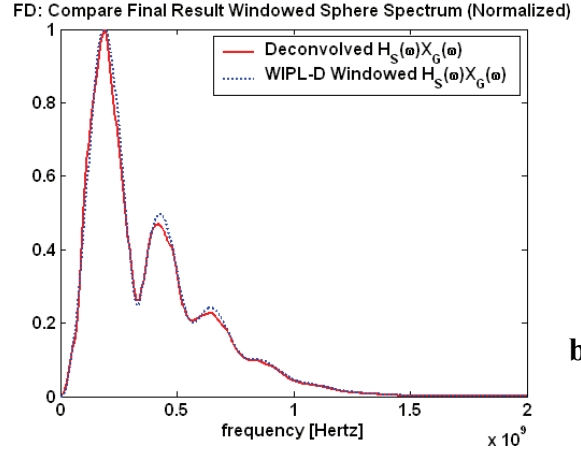


Figure 23 Overlay Deconvolved Spectrum with Direct Simulated Sphere with Input

Now, we will proceed with recovery of the time domain signature. The same process will be used as previously detailed and illustrated in Figures 9 through 12. The same signal processing parameters are used, as shown in Table 2. Since the data is already convolved with the Gaussian input pulse, there is no need to perform additional windowing. Figure 24 plots the real and imaginary spectrum with zero padding and zooms in to show a smooth transition to zero.

Figure 25 plots the inverse Fourier transform of the deconvolved spectrum. This is the recovered time domain signature of the sphere scatterer convolved with the input. Figure 26 overlays this deconvolved time domain signature with the inverse Fourier transform of the direct simulated sphere, previously shown in Figure 17. Again, good agreement is achieved.

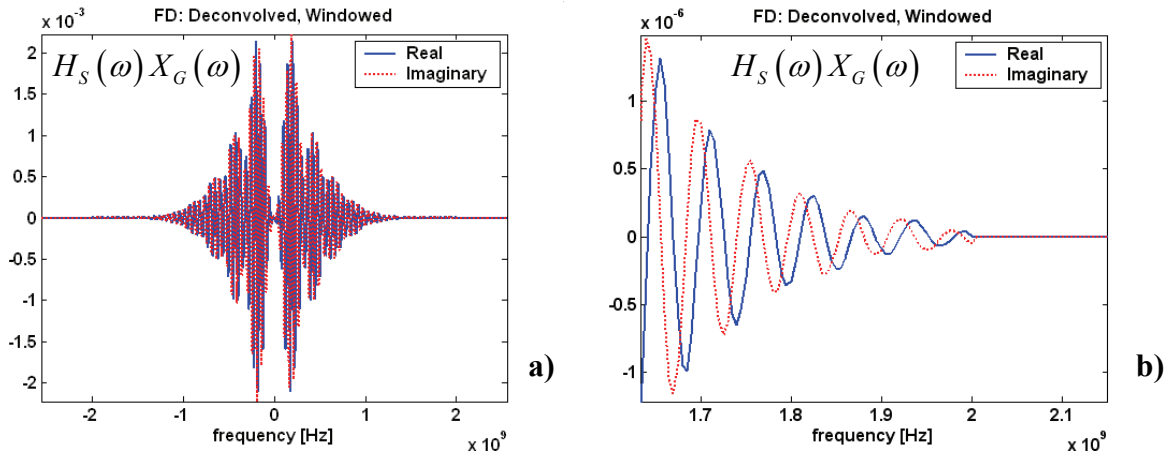


Figure 24 Process the Deconvolved Spectrum to Recover the Time Domain Response: a) Conjugate Symmetry and zero pad (spectrum already windowed), b) zoom in around 2GHz

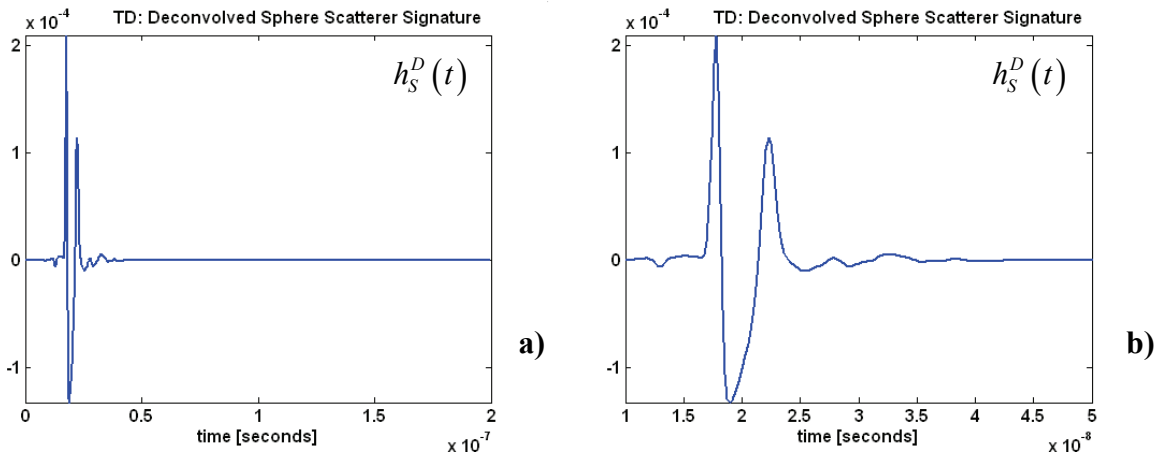


Figure 25 Deconvolved Time Domain Signature of the Sphere Scatterer: a) full time support, b) zoom in on the shape of the Deconvolved Sphere Scatterer Signature

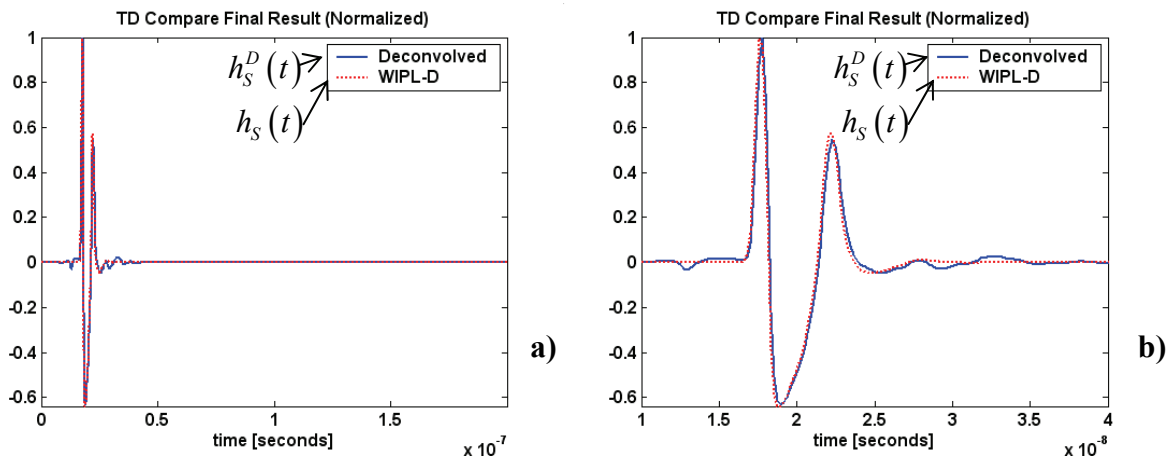


Figure 26 Overlay Deconvolved Sphere Time Domain with WIPL-D Simulated Sphere: a) the full time support, b) zoom in on the shape of the Sphere Time Domain Signature

As an additional check, we synthesize the frequency and time domain responses for the late time pulse (LTP) with no mutual coupling and compare these to the results produced from the simulation of the full bistatic antenna scene with the scatterer, but after isolating the LTP. The process is a convolution of the Gaussian input, the Tx IRA, the sphere scattering and the Rx IRA, represented below, yielding the late time response in frequency: $Y_L(\omega) = \mathfrak{F}\{y_L(t)\}$.

$$X_i(\omega)H_T(\omega)H_S(\omega)H_R(\omega) = Y_L(\omega)$$

Figure 27 overlaps the convolution product before and after including the Gaussian input. Figure 28 shows the normalized frequency domain of the synthesized response overlaid with the results from the simulation of the complete bistatic antenna scattering scene with the sphere, but with the mutual coupling removed. The synthesized spectrum is Fourier transformed to give the time domain response, which is plotted in Figure 29.

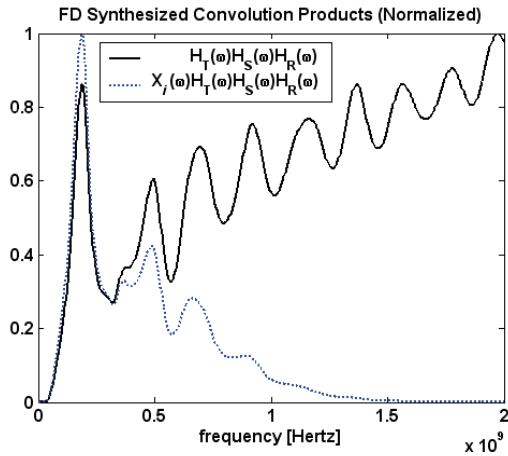


Figure 27 Convolve Scene Components, with/without Gaussian Input (window)

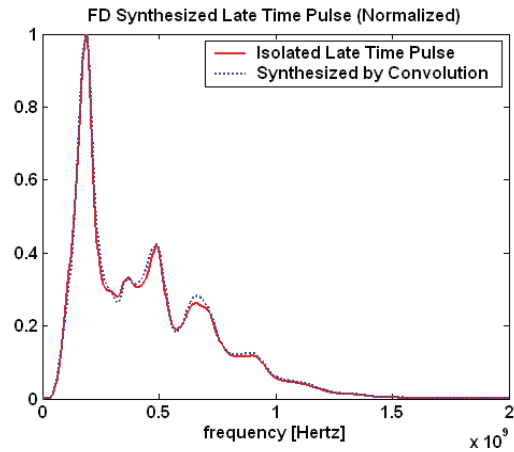


Figure 28 Overlay Isolated LTP with Synthesized Convolution Product

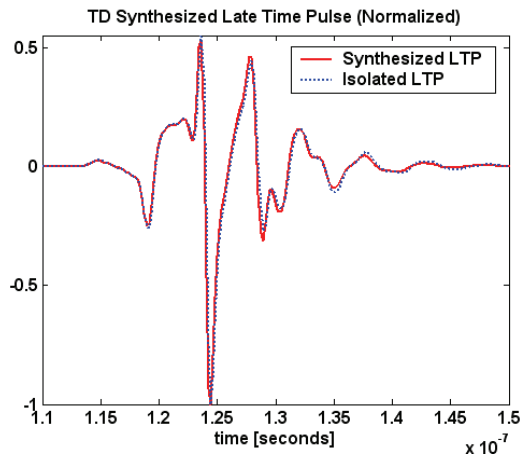
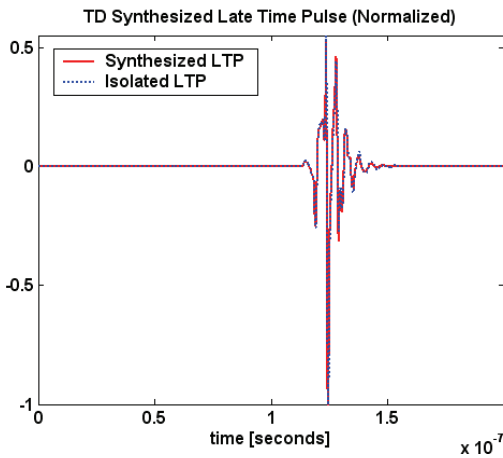


Figure 29 Overlay Convolved Late Time Scene Components with Isolated Late Time Pulse

FUTURE WORK:

Additional work can focus on quantifying the difference between the direct simulated and the deconvolved results, and then experimenting with methods to improve the agreement. Work in progress includes simulating the scene with finer frequency resolution to capture and smooth the high frequency variations observed in the spectrum of the scene with scatterer. Additional simulations are also currently running to try different distances between the bistatic antenna arrangement and the scatterer. Future work could include adding a perfect electrical conducting ground plane to the scene and then, if successful, trying a more realistic dielectric ground plane in the simulations. More complex scatterer shapes and material configurations can be incorporated.

CONCLUSION:

The description and plots provided here illustrate a process for recovering the frequency domain and time domain signature of a scatterer modeled in a scene with a bistatic antenna arrangement and simulated using the electromagnetic analysis code WIPL-D. This investigation used a pair of IRAs for the antennas and a PEC sphere for the scatterer. The process deconvolves the contribution of the antennas to yield the scatterer signature. The deconvolution is performed in the frequency domain and successfully recovers the time domain and frequency domain signature of the sphere from the simulated scene data. The system approach used is detailed and illustrated with plots. Both the time domain and the frequency domain results compared favorably with the results from simulating the scatterer alone. In addition, a process synthesizing the antenna contributions with the input and the scatterer also achieved good agreement with the direct simulation of the scene.

REFERENCES:

- [1] C. E. Baum, "Radiation of Impulse-Like Transient Fields", Sensor and Simulation Note 321, November 1989.
- [2] M. C. Taylor and T. K. Sarkar, "An Electromagnetic Analysis of the 46cm Diameter Impulse Radiating Antenna (IRA)", Syracuse University CEM Lab Report submitted to AFRL, October 1, 2004.
- [3] E. Farr, "IRA-2 Dimensions", Farr Research, Inc. document dated March 15, 2000. This document is provided with minor edits in the Appendix of reference [2] above.
- [4] E. G. Farr, L. H. Bowen, G. R. Salo, J. S. Gwynne, C. E. Baum, W. D. Prather and T. C. Tran, "Studies of an Impulse Radiating Antenna and a Pulse Radiating Antenna Element for SAR and Target Identification Applications", Sensor and Simulation Note 442, March 2000.
- [5] L. H. Bowen, E. G. Farr, C. E. Baum, T. C. Tran and W. D. Prather, "Experimental Results of Optimizing the Location of Feed Arms in a Collapsible IRA and a Solid IRA", Sensor and Simulation Note 450, November 2000.
- [6] E. Farr, "Analysis of the Impulse Radiating Antenna", Farr Research, Inc., Sensor and Simulation Notes 329, July 1991.
- [7] K. Kim and W. R. Scott, Jr., "Numerical Analysis of the Impulse-Radiating Antenna", Sensor and Simulation Note 474, June 2003.
- [8] D. V. Giri, H. Lackner, I. D. Smith, D. W. Morton, C. E. Baum, J. R. Marek, W. D. Prather and D. W. Scholfield, "Design, fabrication, and testing of a paraboloidal reflector antenna and pulser system for impulse-like waveforms", IEEE Trans. Plasma Sci., Vol. 25, No. 2, pp. 318-326, Apr 1997.
- [9] L. H. Bowen, E. G. Farr, D. I. Lawry, "A Dual-Polarity Impulse Radiating Antenna", Sensor and Simulation Note 479, October 2003.
- [10] C. E. Baum and E. G. Farr, "Impulse Radiating Antennas", in H. L. Bertoni (eds.), pp. 139-147 in *Ultra-Wideband, Short-Pulse Electromagnetics*, New York, Plenum, 1993.
- [11] L. H. Bowen, E. G. Farr, C. E. Baum, T. C. Tran and W. D. Prather, "Results of Optimization Experiments on a Solid Reflector IRA", Sensor and Simulation Notes 463, January 2002.
- [12] J. S. Tyo, "Optimization of the TEM Feed Structure for Four-Arm Impulse-Radiating Antennas", IEEE Trans. on Antennas and Propagation, Vol 49, No 4, pp 607-614, April 2001.
- [13] B. M. Kolundžija, J. S. Ognjanović and T. K. Sarkar, "*WIPL-D* (for Windows manual)", Artech House, Norwood, Mass. 2000 (<http://wipl-d.com>).